JOURNAL OF SPACECRAFT AND ROCKETS
Vol. 43, No. 4, July–August 2006

Roll-Rate Stability Limits of Unguided Rockets with Wraparound Fins

G. Liaño* and J. Morote*
National Institute of Aerospace Technology, 28850 Madrid, Spain

The linearized theory of lateral motion of unguided rockets with wraparound fins shows that, unlike planar configurations, they have different roll-rate stability boundaries depending on the roll direction. An analysis of the asymmetry-governing parameters is presented. An operational criterion is developed expressing the roll-rate limits as a function of a factor accounting for the relative effect of the asymmetry terms.

Nomenclature

C_D	=	drag force coefficient
$C_{m\alpha}$	=	pitching moment coefficient slope
$C_{m\beta}$	=	side moment coefficient slope
$C_{mp\alpha}$	=	in-plane Magnus moment coefficient
$C_{mp\beta}$	=	out-of-plane Magnus moment coefficient
$C_{mq}, C_{m\dot{\alpha}}$	=	damping moment derivatives
$C_{mr}, C_{m\dot{\beta}}$	=	cross-coupling damping moment derivatives
$C_{N\alpha}$	=	normal force coefficient slope
$C_{N\beta}$	=	side force coefficient slope
D	=	reference length, missile diameter
g	=	gravity acceleration
I_x, I_y	=	axial and transversal moments of inertia
$K_{j0}e^{i\phi_{j0}}$	=	initial value of modal vectors
m	=	mass
p	=	roll rate
S	=	reference area, $\pi D^2/4$
s	=	nondimensional arc length, $(1/D)\int_{t_0}^{t} V\,\mathrm{d}t$
V	=	speed of missile
α, β	=	angles of attack and sideslip
λ_j	=	damping rates
ξ	=	complex angle of attack, $\beta + i\alpha$
ρ	=	density
ϕ_j'	=	modal frequencies

Subscripts

p	=	equivalent planar fin configuration
w	=	wraparound fin configuration

Introduction

ALMOST every finned projectile is designed to acquire a certain spin. This rotation is intended to reduce dispersion due to manufacturing tolerances. In the absence of spin, the lift produced by the trim angles associated with tolerances will drive the projectile away from its predicted trajectory. On the other hand, the spin rate must be kept low enough to avoid Magnus-moment destabilizing effects. For conventional rockets with planar fins (PF), the mirror symmetry of the configuration establishes a unique maximum roll rate, irrespective of the roll direction.

Many rocket systems employ wraparound fins (WAFs), due to their stowability characteristics for tube-launched ammunition. However, WAFs may present roll reversals when transitioning through Mach 1, significant side forces and moments at angle of attack, and different roll stability derivatives depending on the roll direction, due to the lack of mirror symmetry. The out-of-plane side moment leads to different roll-rate limits, depending on the sense of rotation. This asymmetry can even lead to roll limits of the same sign. In such a case the rocket is unstable at zero spin and must be stabilized with a minimum roll rate in the proper direction.

This paper presents a linear analysis of the roll-rate limits for asymmetric missiles. For a given WAF configuration, the limit values of an equivalent planar fin missile, together with a defined asymmetry factor, can be used to obtain the WAF limits.

Background

The pitching and yawing motion of a missile can be described in terms of the complex angle of attack ξ. The linearized lateral motion of a symmetric missile in free flight is governed by the following differential equation[1]:

$$\xi'' + [H - iP]\xi' - [M + iPT]\xi = P(gD/V^2) \tag{1}$$

where

$$H = C^*_{N\alpha} - 2C^*_D - k_t^{-2}(C^*_{mq} + C^*_{m\dot{\alpha}})$$

$$T = C^*_{N\alpha} - C^*_D + k_a^{-2}C^*_{mp\beta}, \qquad M = k_t^{-2}C^*_{m\alpha}$$

$$P = (I_x/I_y)(pD/V), \qquad k_{t,a} = \sqrt{I_{y,x}/mD^2}$$

$$C^* = (\rho SD/2m)C$$

Equation (1) is expressed in a nonrolling axis system, which yaws and pitches but does not roll with the body (Fig. 1). The independent variable is the nondimensional arc length s.

In comparison with planar fins, WAFs have more complex aerodynamics due to their lack of mirror symmetry. Early work based on wind-tunnel tests[2,3] determined the basic differences between WAF and PF aerodynamics. The static stability derivatives at zero angle of attack of WAFs were essentially the same as with equivalent planar fins. In addition, cross derivatives (out of plane) induced by the curved fins appeared to be significant for Mach numbers above 2.5. By Maple–Synge analysis, Stevens[4,5] showed that WAFs introduced additional stability derivatives, such as $C_{m\dot{\beta}}, C_{mr}, C_{m\dot{\beta}}$, and $C_{mp\alpha}$. He derived the complete differential equation using time as the independent variable. The side effects of WAFs were also investigated by means of aeroballistic range testing.[6–9] It was concluded that designers of such configurations should also consider the possibility of this side moment, because it can have a dramatic effect on trajectory computations based on conventional aerodynamic coefficients and derivatives. Experimental and computational analyses with computational fluid dynamics tools were accomplished[9–11] to investigate the origin of these new derivatives.

Presented as Paper 2005-436 at the AIAA 43rd Aerospace Sciences Meeting, Reno, NV, 10–13 January 2005; received 20 May 2005; revision received 27 September 2005; accepted for publication 12 October 2005.

*Research Engineer, Aerodynamics Division, Carretera de Ajalvir, KM 4, Torrejón de Ardoz. Member AIAA.

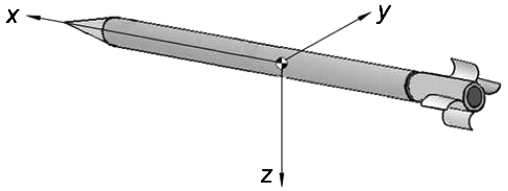

Fig. 1 Nonrolling reference axes.

A complete derivation of the transverse equation of motion utilizing the nondimensional arc length as the independent variable was given in Refs. 12 and 13, including the influence of the out-of-plane side force and moment, the cross-coupling damping moment, and the in-plane Magnus moment. If these additional terms are considered, Eq. (1) transforms into the following expression:

$$\xi'' + [H - i(P - I)]\xi' - [(M + PU) + i(N + PT)]\xi = P(gD/V^2) \tag{2}$$

where the additional WAF coefficients N, I, and U stand for

$$N = k_t^{-2} C^*_{m\beta}, \qquad I = C^*_{N\beta} + k_t^{-2}\left(C^*_{mr} - C^*_{m\dot{\beta}}\right)$$

$$U = -C^*_{N\beta} + k_a^{-2} C^*_{mp\alpha}$$

The general solution of Eq. (2) for steady free-flight conditions is the sum of a constant contribution due to gravity and two modal waves describing the missile response to initial conditions:

$$\xi_j = K_{j0} \exp(i\phi_{j0}) \exp[(\lambda_j + i\phi'_j)s], \qquad j = 1, 2 \tag{3}$$

The initial amplitude and orientation of the modal waves ($K_{j0}e^{i\phi_{j0}}$) are functions of the initial conditions. The dynamic stability requirement is that the damping exponents λ_j be nonpositive throughout the flight of the missile. The damping rates of the motion can be expressed as

$$\lambda_j \approx -\frac{1}{2}\left[H \mp \frac{2(N + PT) - H(P - I)}{\sqrt{(P - I)^2 - 4(M + PU)}}\right] \le 0 \tag{4}$$

Expanding inequality (4), a quadratic stability condition for the gyroscopic roll P is obtained:

$$T(T - H)P^2 + (UH^2 + 2TN - HN + THI)P + (MH^2 + N^2 + NHI) \le 0 \tag{5}$$

In the PF case (N, I, U are zero) this equation yields to symmetric roll-rate limits ($P_1 = -P_2$). For WAF configurations the endpoints P_1 and P_2 are no longer symmetric, because of the linear term. In fact, the side moment can produce a complete change of the dynamic stability picture at supersonic speeds, with P_1 and P_2 having the same sign.[12] The consequence is that, unlike PFs, WAFs can be unstable even at zero roll rate. If this occurs, the rocket must be stabilized with roll in the proper direction.

Stability Plot for Wraparound Fins

A dynamic stability criterion for a symmetric missile is described in Ref. 1, using the gyroscopic factor s_g, and introducing a dynamic stability factor s_d that allows a certain level of damping ($\lambda \ge 0$). The rocket can fly through instability zones where one of the damping rates is positive ($\lambda_j \le \lambda$), provided that the growth of the angle of attack is tolerable:

$$r = 1/s_g = 4M/P^2 \tag{6}$$

$$s_d = 2(T + \lambda)/(H + 2\lambda) \tag{7}$$

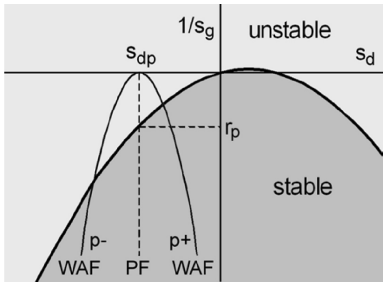

Fig. 2 Stability plot for PFs and WAFs.

For convenience r will be used instead of $1/s_g$. Inequality (4) for planar fins ($N = I = U = 0$) is then equivalent to the following expressions:

$$H + 2\lambda \ge 0 \tag{8}$$

$$r \le s_d(2 - s_d) \tag{9}$$

Inequality (9) defines a parabola in the stability plot (Fig. 2). A rocket below the parabola is dynamically stable, whereas above the parabola it is unstable. The gyroscopic and the generalized dynamic stability factors of Eqs. (6) and (7) can be extended to WAF configurations. Inequality (9) still applies by considering the following expressions:

$$r = \frac{4(M + PU)}{(P - I)^2} \approx \frac{4M}{(P - I)^2} \tag{10}$$

$$s_d = \frac{2\{(T + N/P)[P/(P - I)] + \lambda\}}{H + 2\lambda} \tag{11}$$

For a finned missile P is on the order of 10^{-4}. Hence PU can be neglected in comparison with M. In terms of dynamic stability, the WAF lack of mirror symmetry affects both the gyroscopic and the dynamic stability factors. Except for nonspinning applications, the term I can be neglected in comparison with the gyroscopic roll P. In contrast, the influence of the side moment term N may be dominant if P is small. Expressions (9–11) show that the side moment can destabilize the rocket if it has sufficient magnitude, compared to other aerodynamic coefficients.

In the PF case, a change in roll rate determines a shift along a vertical line in Fig. 2. For missiles equipped with WAFs this is no longer true, because of the explicit dependence in Eq. (11) of s_d on P. To obtain the curve in which a given WAF configuration moves as P changes, we can eliminate P from Eqs. (10) and (11):

$$r = -[(s_d - s_{dp})/A]^2 \tag{12}$$

where

$$A = \frac{N + TI}{(H + 2\lambda)\sqrt{-M}} \tag{13}$$

$$s_{dp} = \frac{2(T + \lambda)}{H + 2\lambda} \tag{14}$$

Equation (12) defines a new parabola in Fig. 2 with a maximum ($r = 0$, $s_d = s_{dp}$) when $p \to \infty$. Each branch of the WAF parabola corresponds to a roll-rate direction. The left branch corresponds to negative values of P, if N is positive. In this case, the right branch is related to positive values of P. The two points of intersection with the neutral stability parabola defined by Eq. (9) yield the gyroscopic roll limits, at which the rocket acquires neutral stability. The WAF parabola degenerates into a vertical line when A is 0 (planar fins). In this case there is only one roll-rate limit, disregarding the roll rotational direction. The presence of a side moment changes this situation, leading to asymmetric roll-rate limits. At the vertex the influence of the side moment becomes zero, and s_d equals s_{dp}.

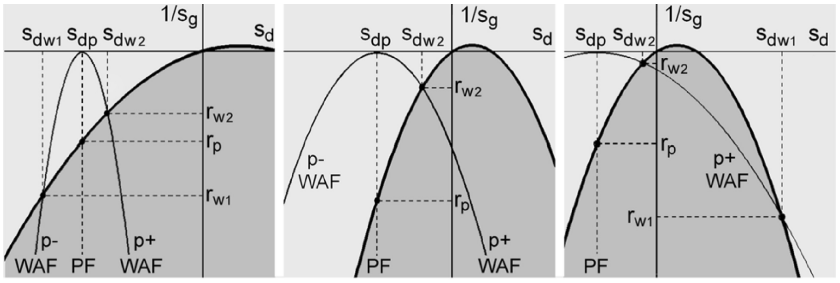

Fig. 3 WAF and neutral stability parabolas.

Equation (14) is the same as Eq. (7); thus s_{dp} is the dynamic stability factor of the equivalent planar fin configuration, which has the same longitudinal characteristics (M, H, T) as the WAF configuration, but all the asymmetry terms (N, I, U) zero. The value r_p in Fig. 2 determines the roll rate at which the planar fin configuration becomes unstable, so it is related to s_{dp} through the expression $r_p = s_{dp}(2 - s_{dp})$. According to Ref. 3, a planar fin missile with the same planform area produces the same lift and pitching moment, but a slightly lower drag, due to the difference in frontal area. Because the drag coefficient makes a minor contribution to H and T, this seems to be a good approximation to the equivalent planar fin configuration. However, the curved fins might produce a significant change of the Magnus moment coefficient, thus altering T. In this respect, much work has been done dealing with Magnus effects on finned missiles,[14–19] but the contribution due to curved fins needs further research. It is well known that WAFs have roll-direction-dependent damping stability derivatives $C_{lp\pm}$. They can also be expected to have roll-direction-dependent Magnus-moment stability derivatives $C_{m\beta p\pm}$ (Ref. 13). They would be amenable to the present treatment by considering two semiparabolas with different vertices.

The size of the parabola (A) is the driving parameter that determines the level of asymmetry of the roll-rate limits. Depending on its value, there are three different situations for the roll-rate stability limits (Fig. 3). For values of A below the unity, the points of intersection lie on different branches of the WAF parabola, and the roll-rate limits have different signs, as in the planar fin case. A critical value occurs when A equals 1. Then the parabolas have the same size and intersect at a unique point. The second point of intersection tends to infinity; that is, one roll-rate limit becomes zero. When A is greater than 1, the points of intersection lie on the same branch of the parabola, so the roll-rate limits have equal signs. An analytical derivation of the points of intersection is included in the Appendix.

Therefore the parameter A determines how the additional aerodynamic derivatives make the rocket depart from the symmetric situation. If the product TI can be neglected, and assuming no damping level (λ), Eq. (13) yields

$$A = N/H\sqrt{-M} \tag{15}$$

Note that the preceding discussion is valid irrespective of the sign of A, because it appears squared in Eq. (12). In the next section, the roll-rate limits are found as a function of this parameter, and then the influence of its sign will be considered.

Roll-Rate Limits

The limits of the gyroscopic roll P can be expressed as functions of A combining Eqs. (11), (13), and (14) and Eqs. (A4) and (A5) in the Appendix:

$$P_{wj} - I = \left(A\sqrt{-4M}\Big/-r_p\right)\left(1 - s_{dp} \mp \sqrt{1 - r_p\Big/A^2}\right) \tag{16}$$

The subscript j takes the value 1 or 2. The curves defined by Eq. (16) are depicted in Fig. 4 for the case $s_{dp} < 0$. When $A \to 0$, the limits approach the following values:

$$P_{wj} - I = \mp\sqrt{4M/r_p} = \mp P_p \tag{17}$$

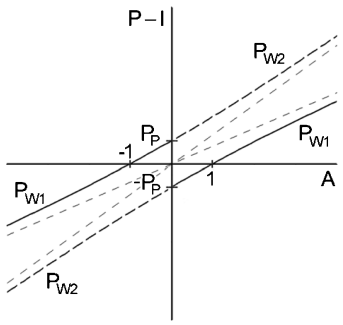

Fig. 4 Gyroscopic roll limits vs factor A ($S_{dp} < 0$).

P_p is the gyroscopic roll for the equivalent PF configuration to achieve neutral stability. Because the limits are odd functions of A, there is a discontinuity when $A = 0$. When $A \to \infty$, the limits tend to the asymptotes $P = m_j A$,

$$m_2 = mP_p, \qquad m_1 = (1/m)P_p \tag{18}$$

where

$$m = +\sqrt{1 - 2/s_{dp}}, \qquad \text{if} \qquad s_{dp} < 0$$

$$m = -\sqrt{1 - 2/s_{dp}}, \qquad \text{if} \qquad s_{dp} > 2$$

Negative values of A, that is, side moments in the opposite direction, change the rotational directions of the limits. The case $s_{dp} > 2$ is similar, the slope of the asymptotes being negative. Within the interval $0 < s_{dp} < 2$, Eq. (16) can produce imaginary solutions. However, real rockets are found[1] to lie outside this interval. A description of this case can be found in the Appendix.

The gyroscopic roll can be scaled with P_p, yielding

$$B_{wj} = (P_{wj} - I)/P_p = \left(A\Big/\sqrt{-r_p}\right)\left(1 - s_{dp} \mp \sqrt{1 - r_p\Big/A^2}\right) \tag{19}$$

In terms of this new parameter, the PF limit $(A \to 0)$ and the asymptotes $(A \to \infty)$ take the simpler values

$$B_{wj} = \pm 1 \tag{20}$$

$$m_2 = 1/m_1 = m \tag{21}$$

For practical purposes the mathematical discontinuities in Fig. 4 do not have any effects, and Eq. (19) provides a roll-rate band where the rocket is stable, as shown in Fig. 5, which depicts the stability boundaries for $s_{dp} < 0$.

For a given Mach number and spin, a rocket is dynamically stable if it lies within the stability band. If the spin varies, while the Mach number is kept constant, the rocket moves along a vertical line (Fig. 5) until it becomes unstable when it reaches B_{w1} or B_{w2}. If the Mach number varies, A and B vary too. Unfortunately, the borderlines also change, because r_p depends on the aerodynamic coefficients through the expression

$$r_p = \frac{4(T + \lambda)(H - T + \lambda)}{(H + 2\lambda)^2} \tag{22}$$

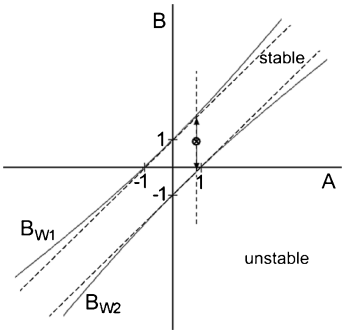

Fig. 5 Scaled roll stability boundaries ($S_{dp} < 0$).

For most cases s_{dp} is far from the interval (0, 2); thus $r_p \ll -1$ and, provided A is in the zone of interest ($|A|$ not much greater than 1), Eq. (19) transforms into

$$B_{wj} = A \pm 1, \qquad \text{if} \qquad s_{dp} < 0$$

$$B_{wj} = -A \pm 1, \qquad \text{if} \qquad s_{dp} > 2 \tag{23}$$

Leaving aside those cases where the Magnus moment is small, and hence s_{dp} is near the interval (0, 2), the borderlines are well represented by straight lines that do not depend on the flight condition. The rocket position in the diagram can be plotted throughout the trajectory and checked with fixed stability limits as long as the requirement $s_{dp} < 0$ or $s_{dp} > 2$ is maintained throughout the flight.

For a given value of A, calculated from Eq. (13) or (15), the curves of Eq. (19) or the straight lines of Eq. (23) determine two limit values B_{wj}, and the corresponding roll-rate limits can be obtained from

$$p_{wj} = (I_y V / I_x D)\left[I + B_{wj}(H + 2\lambda)\sqrt{M/(T + \lambda)(H - T + \lambda)}\right] \tag{24}$$

or

$$p_{wj} = (I_y V / I_x D)\left[I + B_{wj} H \sqrt{M/T(H - T)}\right] \tag{25}$$

if the level of damping λ is taken to be zero. If the small term I is not considered in the analysis, the procedure simplifies even further. In this case, the variable B is the ratio of WAF to PF gyroscopic roll limits (P_w/P_p), but it is also this ratio in terms of the dimensional roll rate (p_w/p_p). If the straight lines of Eq. (23) are to be used, the roll-rate stability limits are readily seen to be

$$p_{wj} = (A \pm 1)p_p, \qquad \text{if} \qquad s_{dp} < 0$$

$$p_{wj} = -(A \pm 1)p_p, \qquad \text{if} \qquad s_{dp} > 2 \tag{26}$$

where p_p is the roll-rate stability limit of the equivalent planar fin configuration. Equation (26) provides a simple relation between PF and WAF limits. Assuming that the equivalent planar fin behavior is known, only the asymmetry factor A of the actual configuration need be calculated to find the stability limits.

Conclusions

This paper presents an analysis of the roll-rate limits for dynamic stability of missiles equipped with wraparound fins. The gyroscopic and dynamic stability factors were extended to WAF configurations so that the dynamic stability criterion based on stability plots could be used. In contrast with the PF case, WAF configurations move along parabolas as the roll rate varies, due to the presence of a side moment, leading to asymmetric roll-rate limits. The size of the WAF parabola is the parameter that determines the level of asymmetry of the stability roll-rate limits.

Expressing the limits as a function of this asymmetry factor facilitates a design tool for roll-rate tailoring along the trajectory. In many cases the limits are well represented by straight lines, which are independent of the flight condition. The stability roll-rate limits of a given WAF configuration are readily obtained from the behavior of the equivalent planar fin configuration by the use of a single parameter.

The characterization of the equivalent planar fin configuration is a matter of research, since WAF configurations can be expected to have roll-direction-dependent Magnus-moment stability derivatives $C_{m\beta p\pm}$, which are amenable to the present treatment by considering two semiparabolas with different vertices.

Appendix: Stability Factors vs A

The roll rates for which a certain rocket acquires neutral stability correspond to those points in Fig. 3 where the WAF parabola intersects with the neutral stability parabola. The analytical expression can be obtained by eliminating $r = 1/s_g$ from Eqs. (9) and (12):

$$s_{dw}(2 - s_{dw}) = -(1/A^2)(s_{dw} - s_{dp})^2 \tag{A1}$$

After a few derivations, the dynamic stability factor of the intersection points can be found:

$$s_{dwj} - s_{dp} = [A^2/(A^2 - 1)]\left[1 - s_{dp} \pm \sqrt{1 - s_{dp}(2 - s_{dp})/A^2}\right] \tag{A2}$$

The subscript j can take the values 1 (plus sign) or 2 (minus sign). Real rockets are found to lie outside the interval $0 < s_{dp} < 2$, the radicand is always positive, and Eq. (A2) yields two real solutions. This expression can be written as a function of r_p, taking into account that r_p and s_{dp} lie in the neutral stability parabola, and so they are related through the following expression:

$$r_p = s_{dp}(2 - s_{dp}) \tag{A3}$$

from which follows

$$1 - s_{dp} = \pm\sqrt{1 - r_p} \tag{A4}$$

Equation (A2) can now be rewritten as

$$s_{dwj} - s_{dp} = [A^2/(A^2 - 1)]\left(1 - s_{dp} \pm \sqrt{1 - r_p/A^2}\right) \tag{A5}$$

or

$$s_{dwj} - s_{dp} = [A^2/(A^2 - 1)]\left(-\sqrt{1 - r_p} \pm \sqrt{1 - r_p/A^2}\right) \quad (\text{if } s_{dp} \geq 1)$$

$$s_{dwj} - s_{dp} = [A^2/(A^2 - 1)]\left(+\sqrt{1 - r_p} \pm \sqrt{1 - r_p/A^2}\right) \quad (\text{if } s_{dp} \leq 1) \tag{A6}$$

The gyroscopic factor of the intersection points can be obtained combining Eqs. (12) and (A6):

$$r_{wj} = -\left\{[A/(A^2 - 1)]\left(-\sqrt{1 - r_p} \pm \sqrt{1 - r_p/A^2}\right)\right\}^2 \tag{A7}$$

This expression is valid for every s_{dp} value; the minus sign is related to $j = 1$, when $s_{dp} \leq 1$. The dynamic and gyroscopic factors are depicted in Fig. A1. When $A < 1$, the second root in the parentheses is greater than the first one, and the two solutions of Eq. (A6) have different signs, corresponding to different branches of the parabola, and hence to different roll rotational directions. When $A > 1$, the first root dominates, and the limits correspond to the same direction of roll rotational speed. In the critical case of $A = 1$, one of the solutions becomes infinite ($P \to 0 \Rightarrow s_{dw1} \to \infty$ and $r_{w1} \to -\infty$) and the other takes the following finite values:

$$s_{dw2} = -s_{dp}^2/2(1 - s_{dp}), \qquad r_{w2} = -r_p^2/4(1 - r_p) \tag{A8}$$

Even though real rockets lie outside the interval $0 < s_{dp} < 2$, it is theoretically possible for a rocket to lie within the interval. In such

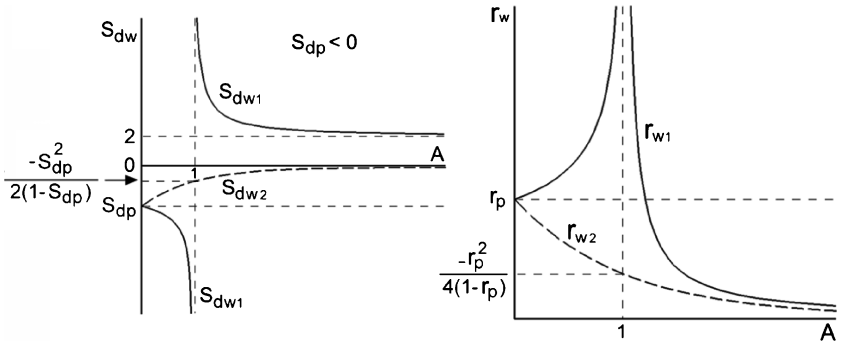

Fig. A1 Dynamic and gyroscopic factors for neutral stability as a function of A.

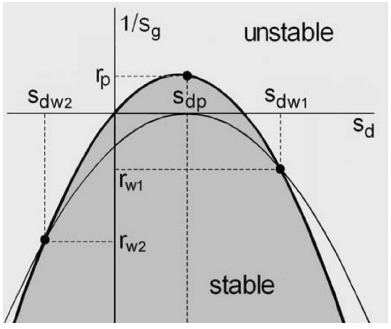

a) Stability plot

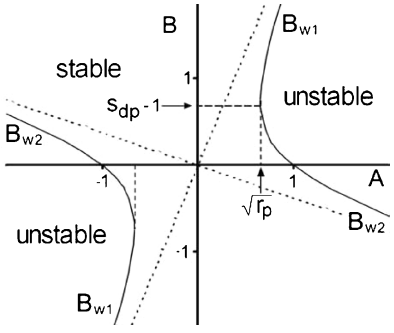

b) Roll boundaries

Fig. A2 Dynamic stability for $0 < s_{dp} < 2$.

a case, the concept of roll limit for the equivalent planar fin configuration does not make sense, because it is always stable. However, the gyroscopic roll can be scaled in a similar way:

$$P_p = \sqrt{-4M/r_p} \tag{A9}$$

The physical meaning of P_p can be seen in Fig. A2, and it is related to the statically unstable configuration having the same s_{dp} value. An expression similar to Eq. (19) applies now:

$$B_{wj} = (P_{wj} - I)/P_p = -\left(A\Big/\sqrt{r_p}\right)\left(1 - s_{dp} \mp \sqrt{1 - r_p\Big/A^2}\right) \tag{A10}$$

The slopes of the asymptotes ($A \to \infty$) have different signs:

$$m_2 = -1/m_1 = -\sqrt{2/s_{dp} - 1} \tag{A11}$$

The stability limits are plotted in Fig. A2b. When $|A| < \sqrt{r_p}$, the two solutions from Eq. (A10) are imaginary, and the rocket is stable for every roll rate. When $|A| > \sqrt{r_p}$, there is a roll-rate band where the rocket is unstable. When $|A| > 1$, the rocket is unstable at $p = 0$ and could be stabilized by roll in any direction.

References

[1]Murphy, C. H., "Free Flight Motion of Symmetric Missiles," Ballistic Research Lab., Rept. 1216, Aberdeen Proving Ground, MD, July 1963.

[2]Dahlke, C. W., and Craft, J. C., "The Effect of Wrap-Around Fins on Aerodynamic Stability and Rolling Moment Variations," U.S. Army Missile Research, Development and Engineering Lab., RD-73-17, Redstone Arsenal, AL, July 1973.

[3]Dahlke, C. W., "The Aerodynamic Characteristics of Wrap-Around Fins at Mach Numbers of 0.3 to 3.0," U.S. Army Missile Research, Development and Engineering Lab., RD-77-4, Redstone Arsenal, AL, Oct. 1976.

[4]Stevens, F. L., "Analysis of the Linear Pitching and Yawing Motion of Curved-Finned Missiles," U.S. Naval Weapons Lab., NWL TR-2989, Dahlgren, VA, Oct. 1973.

[5]Stevens, F. L., On, T. J., and Clare, T. A., "Wrap-Around vs. Cruciform Fins: Effects on Rocket Flight Performance," AIAA Paper 74-777, Aug. 1974.

[6]Winchenbach, G. L., Buff, R. S., Whyte, R. H., and Hathaway, W. H., "Subsonic and Transonic Aerodynamics of a Wraparound Fin Configuration," *Journal of Guidance, Control and Dynamics*, Vol. 9, No. 6, 1986, pp. 627–632; also AIAA Paper 85-0106, Jan. 1985.

[7]Vitale, R. E., Abate, G. L., Winchenbach, G. L., and Riner, W., "Aerodynamic Test and Analysis of a Missile Configuration with Curved Fins," AIAA Paper 92-4495, Aug. 1992.

[8]Abate, G., and Hathaway, W., "Aerodynamic Test and Analysis of Wrap Around Fins with Base Cavities," AIAA Paper 94-0051, Jan. 1994.

[9]Berner, C., Abate, G. L., and Dupuis, A., "Aerodynamics of Wrap Around Fins Using Experimental and Computational Techniques," *Missile Aerodynamics*, RTO MP-5, Paper 7, May 1998.

[10]Tilmann, C. P., Huffman, R. E., Buter, T. A., and Bowersox, R. D. W., "Experimental Investigation of the Flow Structure near a Single Wraparound Fin," *Journal of Spacecraft and Rockets*, Vol. 34, No. 6, 1997, pp. 729–736.

[11]McIntyre, T. C., Bowersox, R. D. W., and Goss, L. P., "Effects of Mach Number on Supersonic Wraparound Fin Aerodynamics," *Journal of Spacecraft and Rockets*, Vol. 35, No. 6, 1998, pp. 742–748.

[12]Tanrikulu, Ö., Önen, C., Mahmutyazicioğlu, G., and Bektaş, İ., "Linear Stability Analysis of Unguided Missiles with Wrap-Around Tail Fins in Free Flight," *Subsystem Integration for Tactical Missiles (SITM) and Design and Operation of Unmanned Air Vehicles (DOUAV)*, AGARD CP-591, Paper 5, Oct. 1995.

[13]Tanrikulu, Ö., and Mahmutyazicioğlu, G., "Magnus Effects on Stability of Wraparound-Finned Missiles," *Journal of Spacecraft and Rockets*, Vol. 35, No. 4, 1998, pp. 467–472.

[14]Benton, E. R., "Supersonic Magnus Effects on a Finned Missile," *AIAA Journal*, Vol. 2, No. 1, 1964, pp. 153–155.

[15]Platou, A. S., "Magnus Characteristics of Finned and Non-Finned Missiles," *AIAA Journal*, Vol. 3, No. 1, 1965, pp. 83–90.

[16]Vaughn, H. R., and Reis, G. E., "A Magnus Theory," *AIAA Journal*, Vol. 11, No. 10, 1973, pp. 1396–1403; also AIAA Paper 73-124, Jan. 1973.

[17]Uselton, J. C., and Carman, J. B., "A Study of the Magnus Effects on a Sounding Rocket at Supersonic Speeds," *Journal of Spacecraft and Rockets*, Vol. 8, No. 1, 1971, pp. 28–34; also AIAA Paper 70-207, Jan. 1970.

[18]Seginer, A., and Rosenwasser, I., "Magnus Effects on Spinning Transonic Finned Missiles," *Journal of Spacecraft and Rockets*, Vol. 23, No. 1, 1986, pp. 31–38; also AIAA Paper 83-2146, Aug. 1983.

[19]Pechier, M., Guillen, P., and Cayzac, R., "Magnus Effect over Finned Projectiles," *Journal of Spacecraft and Rockets*, Vol. 38, No. 4, 2001, pp. 542–549.

M. Miller
Associate Editor